International Journal of Innovation in
Mechanical Engineering and Advanced Materials
Vol. 6 (No. 2). 2024. pp. 67-77
Journal homepage: publikasi.mercubuana.ac.id/index.php/ijimeam
DOI: 10.22441/ijimeam.v6i2.28235

Heat Mapping and Plastic Strain Radius Modeling of Dual-Tool Friction Stir Welds 6061 Aluminum Alloy Plate Using FEM

Rikko P. Youlia [1,3,*], Diah Utami [2,*], Dedik Romahadi [3,4] and Tang Yishuang [1]

[1]State Key Laboratory of Solidification Processing, Shaanxi Key Laboratory of Friction Welding Technologies, Northwestern Polytechnical University, Xi'an, Shaanxi 710072, P. R. China
[2]Department of Industrial Engineering, Universitas Mercu Buana, Jl. Meruya Selatan No. 1, Kembangan, Jakarta 11650, Indonesia
[3]Department of Mechanical Engineering, Universitas Mercu Buana, Jl. Meruya Selatan No. 1, Kembangan, Jakarta 11650, Indonesia
[4]School of Material Science and Technology, Beijing Institute of Technology, Beijing 100811, China
*Corresponding Authors: rikkoputra@mail.nwpu.edu.cn (RP), diah.utami@mercubuana.ac.id (DU)

Abstract

This study investigates the effects of Dual-Tool Friction Stir Welding (DT-FSW) parameters on the weld quality of 8 mm thick 6061 aluminum alloy plates, specifically focusing on the elimination or minimization of the "pass-overlap zone" that's a gap typically observed at the mid-section of the weld cross-section resembling characteristics of the Heat-Affected Zone (HAZ). To address ongoing debates regarding the optimal joint performance concerning this overlap, symmetric increases in the dimensions of both FSW tools were implemented to analyze resultant temperature fields and plastic strain adaptations at the weld interfaces. Simulation visualizations were conducted with tool density variations at intervals of 0.2 mm and 0.4 mm. Results indicate that increasing tool density, thereby reducing the distance between tool surfaces, leads to a decrease in peak temperatures generated during welding. This reduction in temperature correlates with a more uniform distribution of plastic strain rates across all layers of the material—upper, middle, and lower—with the leading edge exhibiting the most significant improvement in strain uniformity. Conversely, during the stabilization phase, a decrease in tool density (S) results in a reduction of the maximum equivalent plastic strain rate. These findings suggest that careful adjustment of tool density in DT-FSW processes can enhance weld quality by promoting more uniform mechanical and thermal properties across the joint.

Article Info:
Received: 9 July 2024
Revised: 22 August 2024
Accepted: 27 August 2024
Available online: 5 September 2024

Keywords:
Double-sided friction stir welding; aluminum alloy 6061; finite element method; nodal temperature; equivalent plastic strain

How to cite:

R.P. Youlia, D. Utami, D. Romahadi, and T. Yishuang, "Heat mapping and plastic strain radius modeling of dual-tool friction stir welds 6061 aluminum alloy plate using FEM," *Int. J. Innov. Mech. Eng. Adv. Mater*, vol. 6, no. 2, pp. 67-77, 2024

1. Introduction

In FSW, the welding process primarily involves a modular tool with non-consumable characteristic that installed in a CNC machine equipped with workpieces configurations. The tool consists of a merged pin and shoulder [1–3] built with a good wearability material then able to rotate and transverse in two directions by an optimized process parameter. The process generates a frictional heat that comes from an axial load pressure and friction of contact between shoulder and workpieces following with mechanical intermixing by the pin, then softens and plasticizes the workpieces within the tool's reach that produces a solid-state joint in less distortion, lower residual stresses and extremely rare fusion-defects [4–8]. And the rotating sides are denoted for the abutting plates as the assembling direction wherein one side suffers from a concordant direction of the rotation with its transverse as the Advancing Side (AS) and the other side suffers a discordant direction of the rotation against its transverse as the Retreating side (RS) [1]. The basic FSW joint technical terminology such as partition of the affected zones, deformation phase and their typical characteristic have been explored by Chekifi et al. [1] and Ning et al. [4]. FSW process is beneficial and credible for welding aluminum alloys due to its advantages compared to fusion welding also the solving solution for welding dissimilar aluminum alloys families [9–11].

Dual Sides Friction Stir Welding or as more popularly known as Double-Sided Friction Stir Welding (DS-FSW) is one of the developed techniques in friction stir-based welding. This technique is an adaptation from the self-reacting technique where it performs more efficient mechanisms than neither of the other derivatives could be performed. DS-FSW is engineered to suit and engage more

thickness variations from medium up to thick plates welding [12] where at these levels of thicknesses the temperature difference is developed [13] that caused by obstruction of heat conduction related to the insufficient distribution of heat generated by shoulder of the tool. Although DS-FSW is highly suitable for welding workpieces with a certain thick, Rahmatian et al. [3] modelled a pass-overlap region schematically or it can be called an inaccessible tool region, especially from the effect of the pin tip and its profile where this region does not have a physical deformation of friction and rotation generated by the tool's pin. Hence this region is predicted as the weakest region, it tends as the adjacent to either the thermomechanical or heat-affected region of the tool's pin. In this case, the pass overlap/tool inaccessible region in the midst gap of two pin's tip has an unique multi-zone partition of inter-affected (point of contact between thermomechanical and heat affected), the materials in this zone do not experience plasticization and its flow formation [14] and several experiment's findings that Low Hardness Zone (LHZ) [15, 16] are discovered in this TMAZ/HAZ boundary due to progressive microstructure enlargement of the metastable S phases [17] and base metal, part of two abutting alloys remains unaffected by the welding process [18]. Moreover, DS-FSW applications for welding thin plates also would face a potential constraint in the tool preparation which is the difficulty of getting the most ideal geometric shape of the pin and its dimensions which will make the pin profile influence become a non-optimal state and probable would tend to as influence on how the form of its identical dynamic motion. The disappearance of the pulsating stirring action [19] during the rotating transformation from static to dynamic motion due to minuscule pin profile might be employed for welding thin plates. Two potential issues have been pointed out which relate to welding aluminum alloys using synergistic DS-FSW where on thin plates the issue comes out to the difficulty of the pin profile-making process in order to achieve the optimal performance when it is placed vertically symmetric (parallel in-line) and the proposing overcome it's to create asymmetrical dislocation and study the asymmetrical distance effect and its ideal intersection. Secondly, investigating the optimal pin length on thick plates over two face-to-face in-line symmetrical tools and the pins feature are taken into account in purpose to reach the pass-overlap zone where no remaining base metal state in the middle layer of weld cross-sectional. The temperature contour and dynamic flow (computational fluid simulation) models and experimental results will be further applied and discussed to those probable trouble-solving.

The fundamental step-by-step welding principle of synergistic DS-FSW is just a copy imitating from the conventional FSW process on the other hand it employs two tools with a specific pin and shoulder profiles one and the same orientated in Y axis where both pin's tip faces are in-confronting and all together rotated, plunged, dwelled, transverse, and retracted back from upper and lower sides in certain process parameters that can be demonstrated in Figure 1 [20–24]. Recapitulation of synergistic DS-FSW application in recent several studies for welding aluminum alloys plates was in the literature list as the reference and theoretical background for the current research to preliminary review its performance, findings, and advantages. In conclusion, the advantages and surpassing limitations of SDS-FSW compared to the conventional DS-FSW method where welding bottom and upper sides alternately that are the SDS-FSW is able to diminish distortion while enhancing welding efficiency, less wear tool's defect and eliminates the need for grinding the initial weld surface to facilitate welding on the opposite side. And compared to the Bobbin tool, SDS-FSW technically has decoupled pins, greater tools life and the speed and rotational direction of both the upper and lower FSW tool can be independently adjusted. This year, there is still a lack of study, development and research regarding the use of SDS-FSW, therefore this research might add to the statistical increase in the number of research search results related to SDS-FSW in the future.

Synergistic DS-FSW has the typical gap in the middle layer of the workpieces on the transverse cross-section area (most of the experiments were done in the working process) where this gap remains unaffected by the tool especially the pin or most similar with HAZ natures. The specific term for this gap is called the "pass-overlap" zone where discussions about this gap are still very hotly discussed among users of the SDS-FSW technique so that the question arises which joint has better performance, whether a joint with pass-overlap or a joint without pass-overlap. Thus, this research will study the metallurgical and mechanical results of welding interfaces without pass-overlap and provide a new perspective for further research. However, it is worth noting that SDS-FSW is often utilized by researchers, for workpiece thicknesses exceeding 6 mm. This leads to speculation regarding its suitability for use on thin plates. Whether reducing the tool dimensions for adapting the size of workpieces will impact its ability to form robust joints where it's speculated earlier that a teensy dimension of the tool might not be giving the best performance. Hence this study will also investigate the application of SDS-FSW, on thin plates.

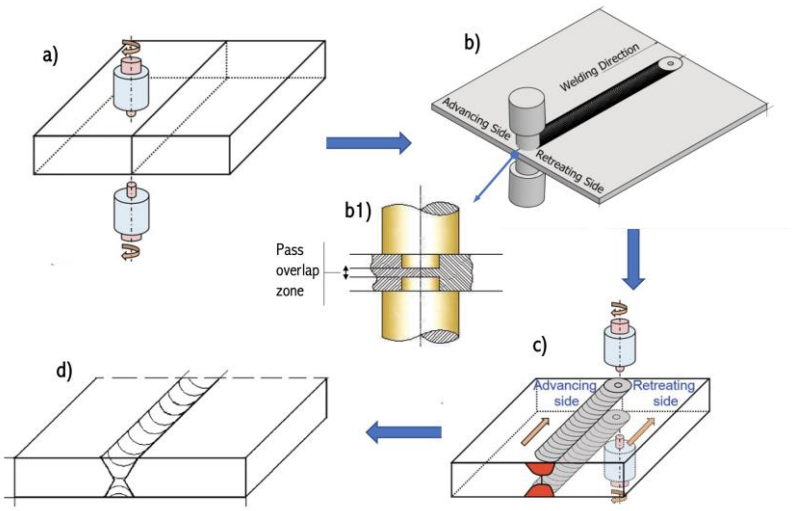

Figure 1. Schematic illustrations of synergistic DS-FSW: a) tools are rotating and dwelling in position; b) plunged and transverse along the longitudinal bonds; b1) vertical display of the plunged tools; c) tools are retracted back; and d) the weld interface.

2. Methods

2.1. Geometry model making (pins and plates)

The tool/chisel model used in this simulation-based research is illustrated in Figure 2. It consists of two parts: the pin and the shoulder. The pin, which is longer than the shoulder, is in the form of a smooth tube, while the shoulder, with a wider diameter than the pin, has an end surface without features. The size of the FSW chisel will be described in the next chapter.

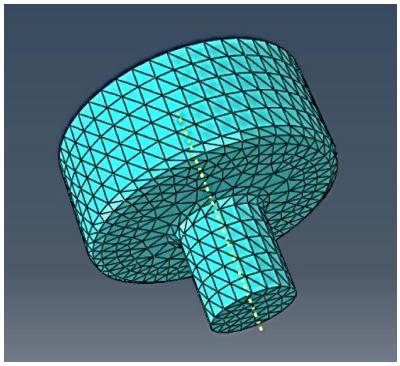

Figure 2. 3D geometrical model of pin.

The Plate/workpiece with a straightforward geometric shape, only a rectangle as described in Figure 3 with dimensions of length x width x height which will be listed in the next chapter. At the stage of adding new material (stage 2), each geometrical part is inputted with data/equation from a material where the tool/chisel refers to Steel H13 or High-Speed Steel (HSS) and the plate to be welded refers to aluminum alloy 6061-xx (Base/Factory Temper adjusts). The specifications of the workpiece, both from the pin and the plate, are tabulated in Tables 1 and 2. The reference data combination of numbers for the material specifications of the tool and plate utilizes the database that the author submitted to the BanuMusa developer.

In this study, there are a total of 2 pins and 2 plates, each with an identical model profile. The process parameters in the simulation range from 1800, 2000, and 2200 rpm for the speed of the FSW moving tool (welding speed) and 1000, 1200, and 1500 for the speed. The matrix combination of process parameters is then run using the bottom-up method.

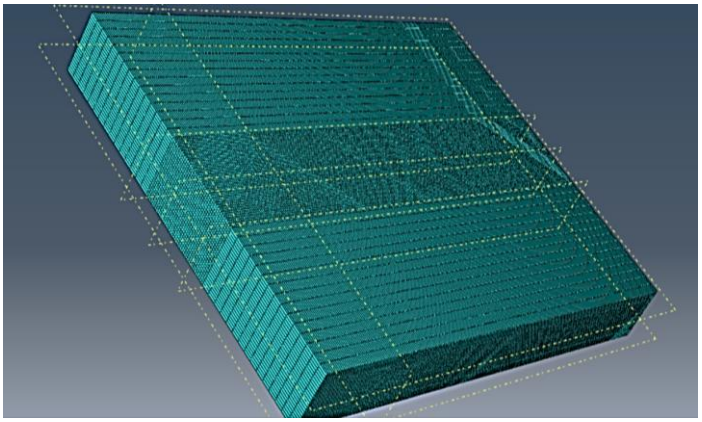

Figure 3. 3D geometrical model of workpiece/plate

Table 1. 6061 aluminum alloy plate specifications for simulation

Description	Values and its unit
Aluminum Alloy 7075	precipitation-hardened wrought aluminum alloys
Workpiece Thermal conductivity	184 W/m K
Workpiece density	2600 kg/m^3
Specific heat of workpiece	1028.25 J/kg K
Elastic Young's modulus	49 x 10^3 N/m^2
Expansion coefficient	2500 1/K
Material solidus temperature	600 K

Note: Values were calculated by JMATPro and units are converted to SI unit.

Table 2. FSW tool specifications for simulation

Description	Values and its unit
Steel	AISI H-13 Tool Steel
Tool density	7850 kg/m^3
Thermal conductivity of tool	45 W/m K
Specific heat of tool	490 J/kg K
Coefficient of friction	0.9

Note: Values were calculated by JMATPro and units are converted to SI unit.

2.2. Meshing and Assembling

The results of meshing for both core parts in this study, the FSW tool and the plate, are presented in Figure 2 and 3. The grid composition on the FSW tool is not yet precise due to the ongoing development of the friction coefficient. The loose grid composition aims to minimize the friction loss between the plate and the tool during the welding process, particularly when the tool moves along the adjacent line/weld interface with specific parameters. On the plate, the grid composition in the welding area (where the pin enters and interacts with the plate) has been reduced to three to four times smaller than the area outside the pin range. This reduction is intended to enhance heat analysis and deformation levels during simulation. The software automatically calculates all previously input data using a specific formula.

The assembly results for 2 chisels and 2 plates are depicted in Figure 4 (top) and Figure 5 (bottom). At this stage of assembly, it also indicates how the working mechanism will operate later during the execution process. It is important to note that the plunging point of both tools is not located at the end or edge of the plate but is instead slightly shifted away from the edge of the plate. This is in accordance with the standard of the FSW process as observed in various studies and applications.

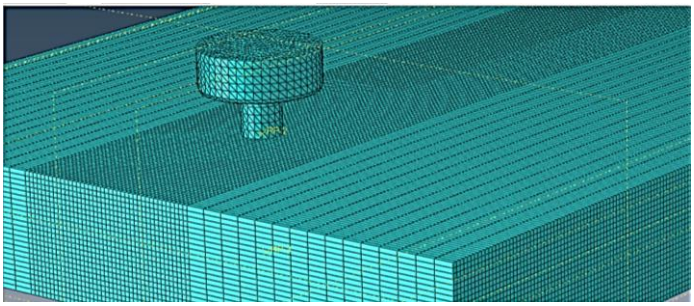

Figure 4. Tool and plate assembled from the top view

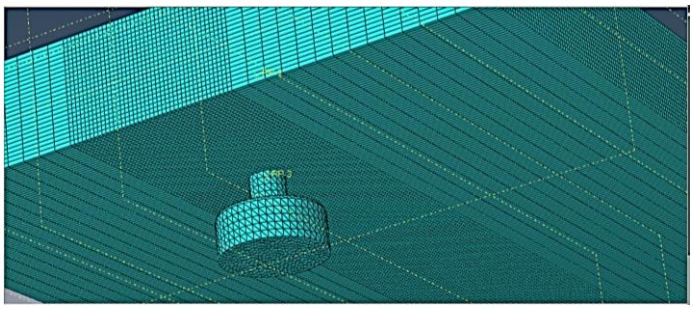

Figure 5. Tool and plate assembled from the bottom view

2.3. Running simulation

When using Abaqus to run a job and analyze results, begin by setting up a job using the "Step" and "Load" modules. Define the analysis steps and specify the load and boundary conditions. Create a job in the "Job" module, name it, and submit it for processing. Monitor the job status in the "Job Monitor" module to address any errors or warnings. Once the analysis is complete, review the results in the "Visualization" module, create plots and reports, and examine the output database for detailed information. Use animation tools for dynamic analysis and verify that the results meet expectations. Evaluate mesh convergence and validate the results against experimental or analytical data if possible. Document findings, adjustments, and insights, and generate a comprehensive report summarizing the analysis setup and results. Maintain an organized and clear model, consider using scripting for automation, and consult the Abaqus documentation for specific details and best practices throughout the process.

2.4. Optimization and validation

In Abaqus, achieving mesh convergence involves creating an initial mesh and setting convergence criteria based on desired parameters like stresses or displacements. After running the analysis, we evaluate the results and identify areas that need improvement. We then refine the mesh iteratively until further changes have minimal impact on the results, indicating convergence. To validate the results, we compare them with experimental or analytical data. This involves establishing validation criteria and running a separate analysis with the refined mesh. We compare the results quantitatively and make adjustments if necessary. It's essential to thoroughly document the process, criteria, and results for a comprehensive assessment of the accuracy and reliability of the FEA model.

3. Results and Discussion

3.1. Concept and geometrical modelling

As of now, there is no existing literature on the simulation model and analysis of synergistic DS-FSW with a minimized middle gap, or in simpler terms, a pass-overlap region. The initial phase of the ongoing research involves simulating the easiest geometric model and mesh processing. The primary objective of this initial experiment is to explore the impact of varying the pin's length on the thermal mechanism. Ultimately, Preliminary experiment has been conducted in simulation way using ABAQUS CAE software that began with increased the pins length in order to fulfil the middle-gap with density variation denoted as “S” at the value of 0.2 and 0.4 in mm. in detail, the S is the gap-distance that measured from face-to-face of pins tip that can be more visible illustrated in Figure 6. The

geometric FSW tool model and its dimension can be drawn in Figure 7 and the tools design has flat featureless shoulder and cylinder shape with no surface feature and then tool's material selected was AISI H-13. The simulation employed a base plate material consisting of aluminum alloy 6061 as the workpiece and organized with a butt configuration to propose a similar joint where the plates dimension was 300 x 100 x 8 in mm units.

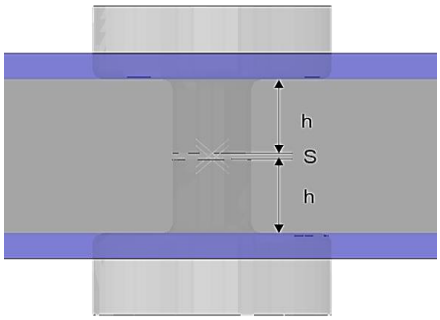

Figure 6. "S" pin tip density in simulative experiments

This model depicts the boundary condition as presented in Figure 8, while Table 1 and 2 outline the physical characteristics of the model and process parameter detail. The model features inlets and outlets on the left and right sides, respectively, with a boundary condition of zero gradient for velocity and pressure. The rotating tool comprises two surfaces referred to as shoulders and pins, with the pin being affixed to the welding material.

Theoretically, During the FSW process, the primary material displacement takes place around the tool shoulder, leading to a division of the workpiece into the flow-capable and non-flow-capable regions. Variable viscosity is specifically applied to the flow-capable region with a designated width, while the non-flow-capable region exhibits dynamic viscosity at a magnitude of 106. The considerably higher viscosity in this region hinders effective flow. AA6061-T6 is treated as a fluid with variable viscosity, specifically assigned to region-2, as depicted in Figure 8. The interface boundaries, segregating the flow and non-flow areas, move at the tool traverse speeds of 1000 - 1500 mm/min. The fluid enters through the inlet during the traverse speed stages and engages with the rotating tool (1800 - 2200 rpm considered for Model-1's parametric study) positioned at the center of the workpiece. This dynamic interaction between the tool and fluid replicates the actual FSW process [25].

3.2. Heat distribution visualization

The visual representation of simulation results through ABAQUS models carries distinct meanings and responses, wherein further discussion and scope focus on the heat generation mechanism, followed by the distributed temperature values and areas experiencing plastic strain during the welding process. In Figure 9, simulative processing illustrates the heat propagation along the weld cross-section area, where the heat source originates from the tool's contact area at the central part of the welding intersection and propagates outward. As the heat intensity diminishes with distance, the temperature decreases, visually represented by shades of green and blue for lower temperatures and shades of yellow-orange and red for higher temperatures.

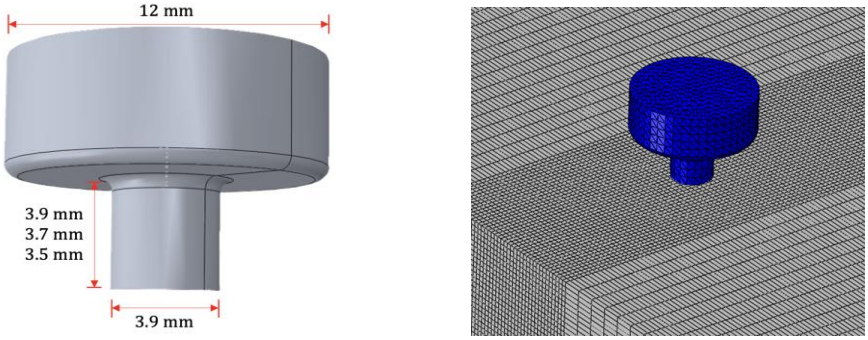

Figure 7. Fabrication model of the chisel/tool used in the initial simulative experiment (model-1) (left), and its net boundary near the weld (right)

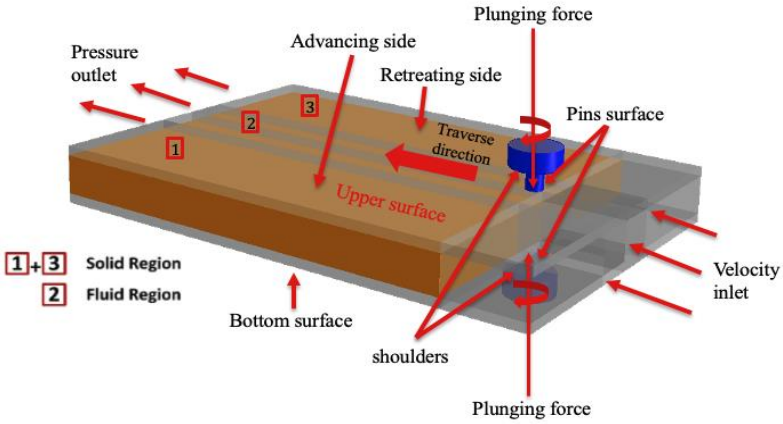

Figure 8. Boundary conditions used in the initial simulative experiment (model-1)

Moreover, it can be visualized in Figure 10 that the distribution of heat is distributed symmetrically on the advancing side and on the retreating side along the welding line. The tool constantly moves at the values at 1800 rpm and 1000 mm.min^{-1} as it is the optimized process parameter and used for both S densities. However, the advancing side experiences a wider and higher temperature grade than the retreating side, this can be shown in Figure 11.

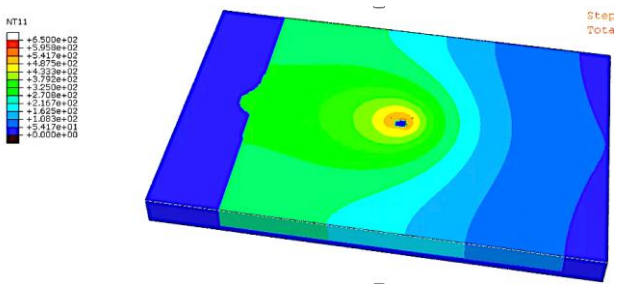

Figure 9. Visual simulation of sources and heat propagation that occur during the welding process

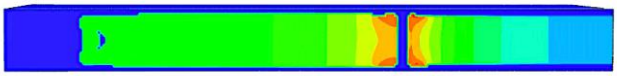

Figure 10. Heat distribution over two sides

The combination of frictional forces and heat conduction occurring during the welding process can result in plastic strain on the material within a specific scope. The range or scope of plastic strain along the traverse cross-section has been successfully predicted, as depicted in Figure 12. Based on the visualization from simulative processing, it can be observed that the range of plastic strain is very small, limited to the dimensions of the tool. Thus, the scope of these plastic strain forces is centralized only in the weld intersection area. In detail, the colors green, yellow, orange, and red represent different levels of the plastic strain rate, with red indicating the maximum rate or nearly perfect deformation.

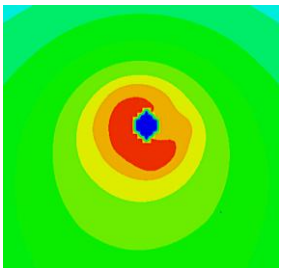

Figure 11. Heat maps around the contacted area of two sides

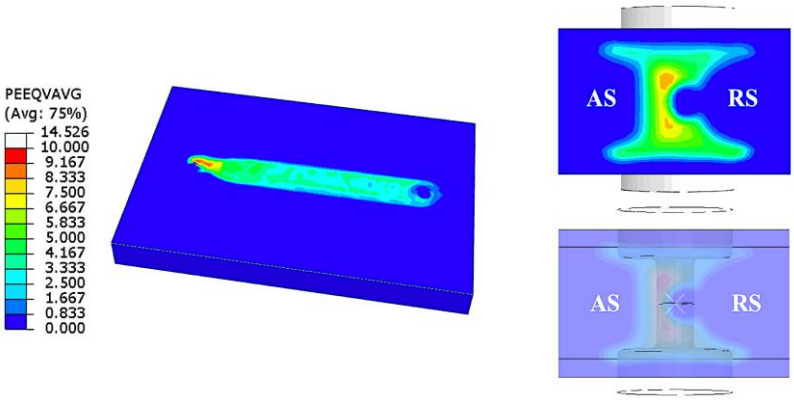

Figure 12. Range and scope of plastic strains

Based on the visualization results of simulation processing, observations were made regarding the density of tools "S" with density intervals of 0.2, and 0.4 mm. It was observed that as the tools' density increases or the gap between the two tool faces decreases, the peak temperature generated becomes smaller, as illustrated in Figure 13.

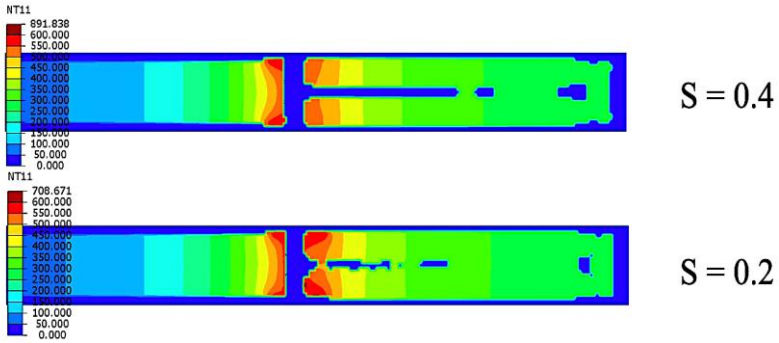

Figure 13. Effect of tool density on peak temperature

Furthermore, in Figure 14, it is demonstrated that the density factor between the two tools also influences the range or scope of plastic strain across all layers (top, middle, and bottom layers). As the density increases, the distribution of plastic strain rate becomes more uniform across all layers. However, the advancing side experiences the greatest benefit from this even distribution of plastic rate. This contrasts with the maximal rate of equivalent plastic strain during the stabilization phase, where the maximum equivalent plastic strain value decreases if the S (density) is also decreased.

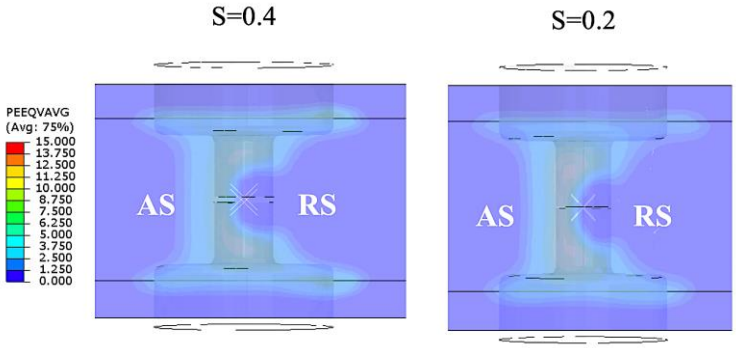

Figure 14. Distribution of equivalent plastic strain in the welded plate during the stabilization phase

3.3. Comparative study of single-tool DS-FSW and double-tool DS-FSW

All the phenomena occurring in the creation and propagation of heat, as represented in Figure 9, align with the principles of physics governing heat generation and the softening mechanism resulting from friction between two objects, either both in motion or one in a stationary state. Specifically,

the heat generated or the change in heat transferred over a specific propagation distance equals the volume of interaction friction between the tool and workpiece (in case of FSW), along with the dimensional ratio of their thicknesses. Besides, during FSW process, heat is generated, and the material undergoes a plasticized state without reaching its melting point as it is a common finding that the heat generation mechanism on the advancing side is often considered more effective than on the retreating side, the most rational is due to unbalance dissimilarity of increased plastic deformation and higher strain rates, because on AS has a mechanism that the tool compresses and stirs the material, inducing greater mechanical work and heat generation then the plastic deformation arises from the intense shearing forces and frictional heat at the advancing interface.

A comparative study between synergistic DS-FSW (dual head) and two-passes DS-FSW (single head) reveals differences in the distribution of plastic strain across the traverse cross-section. According to the simulation result illustrated in Figure 15 (a, b), in the SDS-FSW method (a), the equivalent plastic strain is uniformly distributed, peaking during the initial welding phase. Conversely, the two-passes DS-FSW (b) approach demonstrates a disparity, with the first weld experiencing a higher equivalent plastic strain than the second weld. The maximum strain in the first weld occurs during the initial stage of welding.

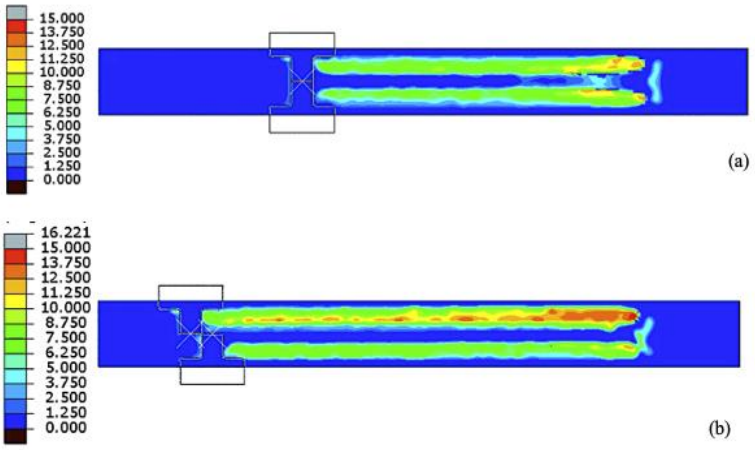

Figure 15. Distribution of plastic strain equivalence in SDS-FSW (a) and two-passes DS-FSW (b) techniques

References Furthermore, it can be visually observed that the welding heat input in synergistic DS-FSW is lower compared to its two-pass counterpart. The primary cause of the variance in welding heat input between the two methods is associated with the grain refinement and residual Cu-alloys particles present in the stirred zone after single-sided welding, hindering the material flow [26] which is the characteristic of two-passes mechanism.

Thermal conditions in the welding process using the FSW technique are one of the two main factors that influence the perfection of deformation. The phase-to-phase changes during the process have a strong chain of relationships and this is the fundamental processes of Friction Stir Welding (FSW) which are intricately linked physical phenomena. In this context, the generation of heat can be traced back to frictional and contact conditions, while the movement of material is reciprocally influenced by this heat generation. In detail, this chain of phase ecosystem changes has been described by Bagheri et al. through the results of their thermal analysis [27]. Yi et al. [28] revealed formula for heat generation under the FSW process, heat stages and heat relationship to a microstructure recrystallization. They concluded that the complexity of the final grain size in the stir zone is intricately influenced by the heat input, however, the average grain size typically rises with the heat input, which is directly tied to variations in welding temperature, this temperature change occurs in three distinct stages: heating, soaking at the peak temperature, and cooling and so the heat input is mainly defined by the peak temperature and cooling rate, with differences in heat inputs attributed to varying cooling rates, ultimately, the final grain size is predominantly determined by the peak temperature.

4. Conclusions

The effect of pins length interval on thermal history during the process of Synergistic DS-FSW aluminum alloy 6061 has been observed. The following conclusions can be drawn from the study that are while the density value of S diminishes (approaching zero), there is a gradual decrease in both

the maximum equivalent plastic strain value of the weld plate and the peak weld temperature, resulting in a reduction of defects. Furthermore, it has been observed that a higher temperature gradient occurs in the forward direction of the welding tool, specifically on the advancing side. Besides, the material's plastic strain is predominantly centered in the central region of the weld, primarily because of the elevated temperature occurring in the direct contact zone of the welding tool, which is positioned at the center. The optimized process parameters used in simulation are 1800 rpm for rotational speed and 1000 mm/min^{-1} for welding speed. In addition, it is Suggested for elevating the complexity geometry model and repairing the configuration of meshing properties can intently open new insight into the design's swept force that might generate and distribute temperature wider and symmetrically.

Acknowledgments

Authors would like to appreciate the facilities and support of Northwestern Polytechnical University. The first author is hoping that academic cooperation can be established in the future between these two affiliations. This research was funded by Mercu Buana University under contract number of 02-5/795/B-SPK/III/2024 in the young lecturer research program category

References

[1] M. Boukraa, T. Chekifi, and N. Lebaal, "Friction stir welding of aluminum using a multi-objective optimization approach based on both taguchi method and grey relational analysis," *Exp. Tech.*, vol. 47, no. 3, pp. 603–617, 2023, doi: 10.1007/s40799-022-00573-6.

[2] N. F. Alkayem, B. Parida, and S. Pal, "Optimization of friction stir welding process using NSGA-II and DEMO," *Neural Comput. Appl.*, vol. 31, no. s2, pp. 947–956, 2019, doi: 10.1007/s00521-017-3059-8.

[3] B. Rahmatian, S. E. Mirsalehi, and K. Dehghani, "metallurgical and mechanical characterization of double-sided friction stir welded thick AA5083 aluminum alloy joints," *Trans. Indian Inst. Met.*, vol. 72, no. 10, pp. 2739–2751, 2019, doi: 10.1007/s12666-019-01751-8.

[4] N. Guo, Y. Fu, Y. Wang, Q. Meng, and Y. Zhu, "Microstructure and mechanical properties in friction stir welded 5A06 aluminum alloy thick plate," *Mater. Des.*, vol. 113, no. 10, pp. 273–283, 2017, doi: 10.1016/j.matdes.2016.10.030.

[5] R. M. Leal and A. Loureiro, "Effect of overlapping friction stir welding passes in the quality of welds of aluminium alloys," mater. des., vol. 29, no. 5, pp. 982–991, 2008, doi: 10.1016/j.matdes.2007.03.018.

[6] K. Umanath, K. Palanikumar, V. Sankaradass, and K. Uma, "Optimizations of friction stir welding process parameters of AA6063 Aluminium alloy by Taguchi technique," mater. today proc., vol. 46, no. 3, pp. 4008–4013, 2020, doi: 10.1016/j.matpr.2021.02.539.

[7] G. Buffa, D. Campanella, A. Forcellese, L. Fratini, U. La Commare, and M. Simoncini, "In-process control strategies for friction stir welding of AZ31 sheets with non-uniform thickness," int. j. adv. manuf. technol., vol. 95, no. 1–4, pp. 493–504, 2018, doi: 10.1007/s00170-017-1223-z.

[8] A. Azadi Chegeni and P. Kapranos, "A microstructural evaluation of friction stir welded 7075 aluminum rolled plate heat treated to the semi-solid state," *Metals (Basel).,* vol. 8, no. 1, 2018, doi: 10.3390/met8010041.

[9] A. E. Abere, A. A. Tsegaw, and R. B. Nallamothu, "Process parameters optimization of bobbin tool friction stir welding on aluminum alloy 6061-T6 using combined artificial neural network and genetic algorithm," *J. Brazilian Soc. Mech. Sci. Eng.*, vol. 44, no. 11, pp. 1–12, 2022, doi: 10.1007/s40430-022-03870-8.

[10] M. V. R. D. Prasad and K. Kumar Namala, "Process parameters optimization in friction stir welding by ANOVA," *Mater. Today Proc.*, vol. 5, no. 2, pp. 4824–4831, 2018, doi: 10.1016/j.matpr.2017.12.057.

[11] J. Sarvaiya and D. Singh, "Selection of the optimal process parameters in friction stir welding/processing using particle swarm optimization algorithm*," Mater. Today Proc.*, vol. 62, pp. 896–901, 2022, doi: 10.1016/j.matpr.2022.04.062.

[12] S. Meng, H. Liu, J. Xiao, T. Huang, Y. Ni, and S. Sun, "A method for process parameter optimization of simultaneous double-sided friction stir welding using a heat transfer model," *Int. J. Adv. Manuf. Technol.*, vol. 121, no. 5–6, pp. 3747–3758, 2022, doi: 10.1007/s00170-022-09544-y.

[13] X. Lu, W. Zhang, X. Sun, S. Sun, and S. Y. Liang, "A study on temperature field and process of FSW thick 2219 aluminum alloy plate," *J. Brazilian Soc. Mech. Sci. Eng.*, vol. 45, no. 6, pp. 1–14, 2023, doi: 10.1007/s40430-023-04254-2.

[14] H. Luo, T. Wu, J. Fu, W. Wang, N. Chen, and H. Wang, "Welding characteristics analysis and application on spacecraft of friction stir welded 2A14-T6 aluminum alloy," *Materials (Basel).,* vol. 12, no. 3, 2019, doi: 10.3390/ma12030480.

[15] Z. Liang, X. Wang, C. Cai, and D. Wang, "Microstructure and mechanical properties of thick plate friction stir welds for 6082-t6 aluminum alloy," *High Temp. Mater. Process.*, vol. 38, no. 2019, pp. 525–532, 2019, doi: 10.1515/htmp-2018-0074.

[16] Y. Hu, H. Liu, S. Li, S. Du, and D. P. Sekulic, "Improving mechanical properties of a joint through tilt probe penetrating friction stir welding," *Mater. Sci. Eng. A,* vol. 731, no. September 2017, pp. 107–118, 2018, doi: 10.1016/j.msea.2018.06.036.

[17] I. Morozova et al., "Precipitation phenomena in impulse friction stir welded 2024 aluminium alloy," *Mater. Sci. Eng. A*, vol. 852, no. January 2022, pp. 1–11, 2022, doi: 10.1016/j.msea.2022.143617.

[18] C. de Souza Carvalho Machado et al., "How microstructure affects localized corrosion resistance of stir zone of the AA2198-T8 alloy after friction stir welding," *Mater. Charact.*, vol. 174, no. February, 2021, doi: 10.1016/j.matchar.2021.111025.

[19] J. Marzbanrad, M. Akbari, P. Asadi, and S. Safaee, "Characterization of the Influence of Tool Pin Profile on Microstructural and Mechanical Properties of Friction Stir Welding," *Metall. Mater. Trans. B Process Metall. Mater. Process. Sci.,* vol. 45, no. 5, pp. 1887–1894, 2014, doi: 10.1007/s11663-014-0089-9.

[20] Hendrato, Jamasri, Triyono, and P. Puspitasari, "Mechanical properties and microstructure evolution of double-sided friction stir welding AA6061-T6," *Key Eng. Mater.*, vol. 935, no. 11, pp. 73–81, 2022, doi: 10.4028/p-08610s.

[21] K. Krasnowskp, P. Sedek, M. Łomozik, and A. Pietras, "Impact of selected FSW process parameters on mechanical properties of 6082-T6 aluminium alloy butt joints," *Arch. Metall. Mater.*, vol. 56, no. 4, pp. 965–973, 2011, doi: 10.2478/v10172-011-0106-9.
[22] I. HEJAZI and S. E. MIRSALEHI, "Effect of pin penetration depth on double-sided friction stir welded joints of AA6061-T913 alloy," *Trans. Nonferrous Met. Soc. China*, vol. 26, no. 3, pp. 676–683, 2016, doi: 10.1016/S1003-6326(16)64158-4.
[23] R. Kumar, S. Varghese, and M. Sivapragash, "A comparative study of the mechanical properties of single and double sided friction stir welded aluminium joints," *Procedia Eng.*, vol. 38, pp. 3951–3961, 2012, doi: 10.1016/j.proeng.2012.06.452.
[24] Y. Zou et al., "A comparative study of microstructure and mechanical properties of conventional and synergistic double-sided FSW joints of 6061 zxaluminium alloy," *Sci. Technol. Weld. Join.*, no. 6, pp. 1–8, 2023, doi: 10.1080/13621718.2023.2227815.
[25] M. Kumar, R. Kumar, and S. D. Kore, "Modeling and analysis of effect of tool geometry on temperature distribution and material flow in friction stir welding of AA6061-T6," *J. Brazilian Soc. Mech. Sci. Eng.*, vol. 44, no. 4, pp. 1–24, 2022, doi: 10.1007/s40430-022-03456-4.
[26] L. A. Bergmann, B. F. Batistão, N. G. de Alcântara, P. Gargarella, and B. Klusemann, "Effect of rotational speed and double-sided welding in friction stir–welded dissimilar joints of aluminum alloy and steel," *Weld. World,* vol. 66, no. 9, pp. 1747–1756, 2022, doi: 10.1007/s40194-022-01333-1.
[27] B. Bagheri, F. Sharifi, M. Abbasi, and A. Abdollahzadeh, "On the role of input welding parameters on the microstructure and mechanical properties of Al6061-T6 alloy during the friction stir welding: Experimental and numerical investigation," *Proc. Inst. Mech. Eng. Part L J. Mater. Des. Appl.*, vol. 236, no. 2, pp. 299–318, 2022, doi: 10.1177/14644207211044407.
[28] D. Yi, T. Onuma, S. Mironov, Y. S. Sato, and H. Kokawa, "Evaluation of heat input during friction stir welding of aluminium alloys," *Sci. Technol. Weld. Join.*, vol. 22, no. 5, pp. 41–46, 2017, doi: 10.1080/13621718.2016.1183079.